Journal of Food Engineering 375 (2024) 112041

Contents lists available at ScienceDirect

Journal of Food Engineering

journal homepage: www.elsevier.com/locate/jfoodeng

# Unravelling temperature-dependent molecular changes in hydrated wheat and maize starches using $^{1}$H time-domain NMR

Jana van Rooyen [a], Leonid Grunin [b], Mecit Oztop [a,c], Danuta Kruk [d], Marena Manley [a,*]

[a] Department of Food Science, Stellenbosch University, Stellenbosch, 7600, South Africa
[b] Resonance Systems GmbH, 28 Seestrasse, Kirchheim Unter Teck, Baden-Wuerttemberg, 73230, Germany
[c] Department of Food Engineering, Middle East Technical University, Ankara, Turkey
[d] Department of Physics and Biophysics, University of Warmia and Mazury in Olsztyn, Oczapowskiego 4, 10-719, Olsztyn, Poland

ARTICLE INFO

*Keywords:*
Starch gelatinisation
Molecular mobility
Proton relaxation
Dry thermal treatment

ABSTRACT

This study proved that time-domain NMR (TD-NMR) experiments can accurately demonstrate the interaction between starch (wheat and maize) and water and the distribution of water molecules in starch-water systems during heating. Molecular properties in starch-water systems at 50% moisture content were monitored by Rhim and Kessemeier – Radiofrequency Optimized Solid-Echo (RK-ROSE) and Carr-Purcell-Meiboom-Gill (CPMG) pulse sequences at frequent (2 °C intervals) measurements during heating (55–80 °C). Starch-like and water-like phases were obtained by RK-ROSE and CPMG pulse sequences, respectively. The second moment, $M_2$, along with the relaxation times of the populations, associated with fast-decaying protons, provided information on the crystal structure state during heating and the extent of gelatinisation. The relaxation times of the most abundant population from the CPMG signal decreased during heating due to strong interactions between starch and water. Temperature of stabilisation of this population aligned with the associated findings from the differential scanning calorimetry and rheological measurements.

## 1. Introduction

Starch is the major component of wheat flour which structurally contribute to baked products, provide gelling in semi-solid foods and serve as a source of complex carbohydrates. Starch granules are characterised by concentric growth rings of which each is composed of blocklets. These blocklets, in turn, contain an arrangement of crystalline and amorphous lamellae. The crystalline region shows a double helical organisation of external amylopectin polymer chains (Bertoft, 2017). This unique arrangement contributes to the functional versatility of starch. Typically, wheat and maize starch contains 25% amylose and 75% amylopectin (Shi et al., 1998; Kim and Kim, 2021).

Hydration of starch involves the heterogeneous diffusion of water molecules into the amorphous regions and establishment of hydrogen bonds with –OH groups of glucose units (Vamadevan and Bertoft, 2020). This interaction leads to reversible granular swelling. Upon further heating above the glass transition temperature, the crystalline regions within the starch granules destabilise, leading to an irreversible loss of molecular order, the melting of crystallites and the subsequent loss of birefringence (Delcour and Hoseney, 2010). Initial gelatinisation occurs in the amorphous regions due to weakened hydrogen bonds in these regions. The extent of gelatinisation is affected by water content and temperature. As water acts as both plasticiser and solvent, the molecular interaction of starch polymers with water is important to be controlled during processing of starch-rich products.

In recent years, various dry thermal treatment techniques have been implemented for modification of wheat flour and starch to extend its utilisation (van Rooyen et al., 2022). Physical modification of the wheat grain by heat treatment may improve the physicochemical, structural and functional properties of the resultant flour (Schoeman and Manley, 2019) and/or starch. Forced convection roasting has attracted increasing attention for wheat processing as it is considered as a safe and energy efficient dry thermal treatment technique (Schoeman et al., 2016). ANOVA-simultaneous component analysis (ASCA) of the shortwave-infrared (SWIR) spectra of whole wheat flour revealed significant changes in its chemical structure after forced convection roasting. The spectral features contributing to these changes were systematically characterised and assessed for statistical significance (van

* Corresponding author.
*E-mail addresses:* 20783353@sun.ac.za (J. van Rooyen), mobilenmr@hotmail.com (L. Grunin), mecit@metu.edu.tr (M. Oztop), danuta.kruk@uwm.edu.pl (D. Kruk), mman@sun.ac.za (M. Manley).

https://doi.org/10.1016/j.jfoodeng.2024.112041
Received 15 September 2023; Received in revised form 1 March 2024; Accepted 10 March 2024
Available online 16 March 2024

Rooyen et al., 2023c). When the same roasting technique was applied. van Rooyen et al. (2023a) observed slight damage to the starch granules and a reduction in the relative crystalline of the flour when wheat was roasted at 115 °C for 165 s compared to an unroasted sample.

Time-domain nuclear magnetic resonance (TD-NMR) reveals the motion of protons ($^1$H) by interpretation of two separate processes, i.e., longitudinal, or spin-lattice relaxation ($T_1$) that involves transfer of energy between spin systems and the environment, and transverse or spin-spin relaxation ($T_2$) which are entropic processes that involves dephasing of nuclear spins. Spin-spin relaxation is more appropriate for analysis of complex food samples as it is less time-consuming and enables easier identification of different proton populations that exist within a sample (Bosmans and Delcour, 2017).

$^1$H TD-NMR has been exploited for understanding water distribution and starch-water interaction when determining the molecular mobility of starch suspensions at water activities from 0 to 0.93 (Choi and Kerr, 2003), and during assignment of proton populations in unheated and heated model systems at 47% water content (Bosmans et al., 2012). Gelatinisation mechanisms upon heating from 20 to 90 °C (with 5–10 °C increments) of hydrated tapioca starch (Rakhshi et al., 2022) as well as wheat, waxy maize and potato starch (Rondeau-Mouro et al., 2015; Kovrlija et al., 2020) have been investigated with a combination of free induction decay (FID) and Carr-Purcell-Meiboom-Gill (CPMG) pulse sequences at intermediate moisture contents (45–50%). Riley et al. (2022) further elaborated on the use of TD-NMR for investigation of proton dynamics in starch rich foods in a comprehensive review.

FID, which is based on a single 90° radiofrequency pulse, is often used for detection of solid crystalline and glassy phases with fast molecular mobility (van Duynhoven et al., 2010). While using such basic sequence, signal from solid components (or fast decaying protons) may be lost due to the probe dead time that interferes with the signal from strong $^1$H–$^1$H dipolar interactions in solid materials (Grunin et al., 2019). Therefore, alternative sequences such as solid-echo (SE), mixed magic-sandwich-echo (MSE) and Rhim and Kessemeier – Radio-frequency Optimized Solid-Echo (RK-ROSE) pulse sequences have been developed to refocus the initial part of the FID signal to avoid dead time issues and allow for detection of signal from solid materials (Maus et al., 2006). Garcia et al. (2019) found RK-ROSE to have a higher efficiency on recovering $^1$H signals from rigid components at short and intermediate echo times compared to SE and MSE.

With regards to NMR signal processing of the FID, typically an Abragam sinc fitting function is applied to obtain the transverse relaxation time (Riley et al., 2022). However, due to the non-exponential, and sometimes oscillating decay of the FID signal from semicrystalline structures, interpretation of the signal fundamentally cannot provide $T_2$ times in their classical interpretation as the exponent parameter. This is because the relaxation time of the fast decaying protons ($T_{2(1)}$) (Garcia et al., 2019) is not in actual fact the period at which the signal magnitude decays in *e* times, as the signal falls faster due to the Sinc envelope. Instead, a distinct $T_2$ or $T_2$* value is provided, while the relaxation time of the CPMG signal is denoted as $T_2$. SE, MSE and RK-ROSE facilitate the recovery of strong dipolar interactions (Garcia et al., 2019). By focussing only on the fast-decaying section, valuable information into the ratio of crystalline to amorphous within starch semicrystalline structures can be obtained. The use of the second moment provides information on the mobility of strong dipolar interactions of rigid protons, which works independent of the shape of the fitting function (Grunin et al., 2019).

In the present study, TD-NMR experiments were applied to hydrated starch, isolated from unroasted and roasted wheat, as well as maize starch. The study aimed to investigate and interpret the $^1$H NMR signal obtained from different starch-water systems at intermediate moisture contents during heating to (1) provide fundamental knowledge on the proton population distribution during gelatinisation; (2) differentiate between starch isolated from roasted and unroasted wheat as well as maize; and (3) compare TD-NMR results with rheological and thermal analysis methods.

## 2. Materials and methods

### 2.1. Sample materials and dry thermal treatment of wheat

A commercial hard wheat cultivar (SST 875) was obtained from SENSAKO (part of the Syngenta South Africa (Pty) Ltd group of companies, Bethlehem, South Africa). Two whole wheat (500 g) samples were roasted in a forced convection roaster (Roastech, Bloemfontein, South Africa) at two optimum conditions to (1) maintain protein quality (108 °C for 130 s) (van Rooyen et al., 2023b) and (2) improve flour viscosifying properties (115 °C for 165 s) (van Rooyen et al., 2023a). Samples prepared from wheat roasted at these conditions will further be referred to as low roasting conditions, RLow (108 °C for 130 s) and high roasting conditions, RHigh (115 °C for 165 s). Unroasted wheat served as the control. Roasting in forced convection roasters are done by continuously rotating an insulated drum containing the sample, to steady temperature control and facilitate uniform thermal treatment. Maize starch was included in this study as an alternative cereal starch with similar amylose to amylopectin ratios as wheat starch. Furthermore, maize was added to also see whether differences between cereal starches could be detected with in the NMR results could be detected.

### 2.2. Starch isolation

Prior to starch isolation, the roasted and unroasted whole wheat kernels were tempered to 15% moisture content (AACC method 26–95.01, AACC International, 2010) and dry milled using a Brabender Quadrumat Jr. (Quadruplex) mill (C.W. Brabender Instruments, South Hackensack, NJ, USA) (AACC method 26–50.01, AACC International, 2010) to separate bran and germ from the endosperm which was recovered as flour. Starch was isolated from the produced white flour using the dough ball method as described by Pauly et al. (2012) with slight modifications. A viscoelastic dough (60% hydration) was formed by mixing 125 g of flour (15% moisture content) with 64 mL of deionised water and allowed to rest for 30 min. The dough was washed with deionised water (*ca.* 600 mL) until washing water was clear to separate the starch from gluten. The starch slurries were filtered through a 180 μm brass sieve, followed by a 45 μm brass sieve, the filtrate was centrifuged at 3500×*g* for 15 min, and the supernatants were discarded. The remaining starch pellets were washed twice with deionised water (*ca.* 200 mL), the supernatants were discarded after each washing and the upper layer of the pellet were removed with a spatula. The obtained starch samples were subsequently freeze dried (VirTis, United Scientific, Cape Town, South Africa) until approximately 10% moisture content and sealed until further analysis.

### 2.3. Rheological properties

Oscillatory rheological measurements of starch-water models were made with the temperature sweep test using a rheometer (Kinexus Dynamic Rheometer, Malvern, Worcestershire, U.K.) equipped with a parallel plate system, at a 1 mm gap. The strain and frequency were respectively set at 2% and 1 Hz. Starch-water samples, hydrated to 50% moisture content, was loaded onto the ram of the rheometer (enough sample to cover the area of the parallel plate) and covered by the hood to prevent moisture evaporation during analysis. The samples were heated from 35 to 90 °C at a rate of 5 °C/min. The viscoelastic modulus (complex modulus, G*) and loss factor tan δ, as the ratio of viscous modulus to elastic modulus (tan δ = G''/G'), were determined. A fresh sample was prepared before each measurement. For each sample (control, RLow and RHigh), measurements were performed in triplicate.

### 2.4. Differential scanning calorimetry

The thermal properties of the starch samples were characterised by differential scanning calorimetry (DSC, Q2000, TA instruments, New

Castle, DE, USA). Starch powder samples (3 mg) were hydrated to 50% moisture content, and hermetically sealed in an aluminium pan. After equilibration at 25 °C for 4 h, the samples were scanned from 25 to 90 °C at a heating rate of 5 °C/min. An empty hermetic aluminium pan was used as a reference. The resulted thermograms were analysed using the Origin 9 software programme (OriginLab Corporation, Northampton, MA, USA). DSC measurements were performed in triplicate for the control, RLow and RHigh starch samples.

### 2.5. Relaxation time measurements by TD-NMR

$^1$H TD-NMR experiments were conducted using an 18.4 MHz benchtop TD-NMR system (Spin Track, Resonance Systems GmbH, Kirchheim unter Teck, Germany) equipped with a 10 mm radio-frequency coil. A variable temperature sample controller was used to regulate heating and cooling of the sample. Heated air that flows around the sample tube were used to heat the sample while NMR measurements were performed. The starch samples (*ca.* 0.25 g) were prepared by hydrating them to 50% moisture content in a 10 mm NMR tube. The starch-water water mixture was mixed with a stirrer, followed by 15 min hydration and stabilisation period prior to analysis. The NMR tube was sealed with a Teflon lid to prevent moisture evaporation during the experiment. RK-ROSE and CPMG pulse sequences were used to respectively determine the solid-like (starch-like) and liquid-like (water like) molecular fractions of the starch-water system during temperature increase. The heating rate of the system was set at 1 °C/min increase, from 20 to 80 °C. Measurements were taken every 10 °C intervals from 20 to 50 °C and every 2 °C intervals from 55 to 80 °C. The temperature controller ensured the system reached the desired temperature before signal acquisition. The total measurement time was *ca.* 120 min for each sample. Transverse relaxation curves were obtained at each specified temperature by simultaneously recording the signal produced by RK-ROSE and CPMG pulse sequences. The probe dead time was 12 μs and the acquisition time for RK-ROSE sequence was set to 0.5 μs. For CPMG sequence, the echo time was set to 1 ms and 200 echo amplitudes were recorded. For all measurements, it was ensured that the repetition time was >5x$T_1$ (2.2 s for the hydrated fresh samples) and 32 scans were used to increase the signal-to-noise ratio. A fresh sample was prepared prior to each measurement. All NMR measurements were performed in duplicate for the control, RLow and RHigh starch samples.

### 2.6. NMR data analysis

Data analysis was conducted using the Relax8 software programme (Resonance Systems GmbH, Kirchheim/Teck, Germany) with the specialised 'Solid Lab' module. The signal obtained from the RK-ROSE sequence are associated with the solid-like (starch-like) phase of the starch-water system. Two data analysis approaches were followed.

(1) Firstly, time dependent changes in the signal, $S(t)$ were fitted with a mathematical model. The function decomposes the curves obtained for hydrated starch system into three components (in terms of the time scale of the molecular motion), according to Eq. (1) (Garcia et al., 2019).

$$S(t) = A_1\, exp^{-\left(\frac{t}{T^*_{2(1)}}\right)^2} \cdot \frac{sin(bt)}{bt} + A_2\, exp^{-\left(\frac{t}{T^*_{2(2)}}\right)^{v_i}} + A_3\, exp^{-\left(\frac{t}{T^*_{2(3)}}\right)^{v_m}} \quad (1)$$

where $A_1$, $A_2$ and $A_3$ respectively indicates the amplitudes of the signal components associated with three components. $T^*_{2(1)}$, $T^*_{2(2)}$ *and* $T^*_{2(3)}$ denotes the corresponding observed spin-spin relaxation times, and $v_i$, and $v_m$ are the respective shape parameters.

(2) In the second approach, the *second moment approximation* (SMA) was applied to the RK-ROSE signal to provide information on the amplitude (strength) of the dipolar interactions between $^1$H nuclei belonging to the semicrystalline (crystalline and amorphous) fraction of the system (Grunin et al., 2019). In other words, the second moment, $M_2$, provides information on the contribution of the crystalline compared to amorphous regions for fast-decaying protons. $M_2$ is based on direct integration of the fast Fourier transform (FFT) of the frequency domain NMR spectrum. Prior to FFT, the contribution of the more mobile fraction (>64 μs) was removed to eliminate signal from mobile segments in the heterogenous samples. The $M_2$ values were calculated according to Eq. (2) (Grunin et al., 2019).

$$M_2 = \frac{\int_{f_{low}}^{f_{high}} x^2 S(x) dx}{\int_{f_{low}}^{f_{high}} S(x) dx} \quad (2)$$

where $S(x)$ was the amplitude spectrum density, and the integration ranges $f_{low}$ and $f_{high}$ were selected as −300 and 300 kHz respectively to maximally embrace most of the informative NMR spectrum.

Strictly speaking, the $T_{2(1)}$ in the first term in Eq. (1) does not refer to a classical relaxation time, since the exponent is multiplied by the decreasing *Sinc* function, and the moment when the signal decays in *e* times happens earlier than $T_{2(1)}$. During fitting, $T_{2(1)}$ will be higher than the *true observable* relaxation time. Hence, $T_2$* is denote as the true relaxation time in all considerations below.

Furthermore, Gaussian and Abragamian functions both have only even terms in their Taylor series expansion (Grunin et al., 2023). Thus, by referring to the second moment alone, it is possible to align $M_2$ from Abragamian (Eq. (1)) (that does not have a classically defined $T_2$), and the $M_2$ of a Gaussian function, ($T_2$ is obtained directly). Thus, within the frame of such *second moment approximation* the observed $T_2^*$ can be expressed by means of the experimentally measured $M_2$ (Eq. (2)) according to Eq (3).

$$T_2^* = \sqrt{\frac{2}{M_2}} \quad (3)$$

CPMG data (liquid-like/water-like phase) of the starch-water systems were fitted to three components of the exponential fitting using Eq. (4).

$$y(t) = A_A\, exp^{\left(\frac{-t}{T_{2(A)}}\right)} + A_B exp^{\left(\frac{-t}{T_{2(B)}}\right)} + A_C\, exp^{\left(\frac{-t}{T_{2(C)}}\right)} + A \quad (4)$$

where $A_A$, $A_B$ and $A_C$ respectively indicate the amplitudes associated with each component for the liquid-like phase. $T_{2(A)}$, $T_{2(B)}$ *and* $T_{2(C)}$ denotes the spin-spin relaxation times. Characteristic RK-ROSE and CPMG decaying curves of a hydrated starch at 20, 40, 55, 65 and 80 °C are shown in Fig. S2, illustrating the change in relaxation behaviour during heating.

### 2.7. Statistical analysis

Analysis of variance (ANOVA) was performed using Addinsoft XLSTAT version 2022.3.1 software (New York, NY, USA). Rheological and thermal property results are presented as mean ± standard deviation of triplicate determination. NMR results are presented in graphical format as means of duplicate analysis with standard errors shown as error bars. Fisher's (LSD) comparison test at a 95% confidence interval was performed to determine significance when necessary.

## 3. Results and discussion

### 3.1. Thermal analysis

The thermal behaviour of the hydrated starch samples was measured by means of a rheometer and DSC. Characteristic thermograms are shown in Fig. S1. Typically, a sharp endothermic peak is observed when starch is completely gelatinised. In this study the endothermic peaks did not show any sharp distinct peaks, therefore the starch was not completely gelatinised. No significant differences ($p > 0.05$) were

observed for the gelatinisation-related temperatures between the wheat samples, obtained with DSC (Table 1). Irrespective of dry heat treatment conditions, the wheat starch samples gelatinised at similar temperatures with onset at approximately 55 °C, peak at 62 °C and final temperatures at 67 °C. The gelatinisation temperatures (onset, peak and final) of the maize starch were found to be significantly ($p < 0.05$) higher compared to the wheat control and dry heat-treated starch samples. This observation aligns with findings in the published literature (Delcour and Hoseney, 2010). Nevertheless, the significantly ($p < 0.05$) lower enthalpy values for RHigh compared to the other samples confirms a certain degree of starch damage resulting from the roasting process. Although not significantly different, the maize starch had the highest enthalpy values. This suggests that more energy is required for the transition from an ordered to a disordered state (Delcour and Hoseney, 2010) in the starch-water mixture.

The complex modulus (G*) measures the overall resistance to deformation of a sample (Kulkarni and Shaw, 2016), indicating the characteristic maximum structural stiffness reached during a constant temperature ramp. The onset of the initial increase of G* reflects initiation of gelatinisation, i.e., starch granule swelling due to increased water absorption (Fig. 1). The temperature at the onset of the initial increase of G* for the wheat samples aligns closely with the temperatures observed for $T_o$, as measured by DSC (Table 1). For maize starch, the temperature associated with the initial G* increase was slightly lower compared to, possibly attributed to its shear-thickening behaviour (Kilbride et al., 2019) and likely influenced by the 2% strain applied during analysis. The impact of temperature dependence on the viscoelastic behaviour of the starch-water systems was more pronounced than the influence of shear. Consequently, the shear was kept constant during the measurement. The effect of temperature can therefore clearly be seen by the increase and decrease in G* (Fig. 1).

At 50% moisture content, the wheat starches exhibited viscoelastic solid characteristics ($\tan \delta < 1$) from *ca.* 50 °C onwards. In contrast, maize demonstrated dominant viscoelastic liquid behaviour ($\tan \delta > 1$) up to 68 °C, transitioning to a more solid-like behaviour thereafter. The shear thickening, and therefore viscoelastic, properties (measured under stress) of starches of different origins vary due to different physical properties, such as molecular size, composition and particle surfaces (Kilbride et al., 2019). With the constant shear strain of 2% applied during analysis, wheat and maize starch exhibited different viscoelastic properties. Therefore, the maximum stiffness observed for the maize and wheat starches cannot be compared. Nevertheless, the RHigh sample showed the lowest values for G* at peak conditions compared to the other wheat samples, suggesting that roasting increased its viscosifying properties (greater softness) (Fig. 1).

**Table 1**
Gelatinisation related temperatures (onset, peak and final) and enthalpy measured by differential scanning calorimetry (DSC) as well as the temperature of initial increase in complex modulus during heating for the starch-water systems at 50% moisture content.

| Sample | $T_o$ | $T_p$ | $T_f$ | ΔH | Initial G* increase |
|---|---|---|---|---|---|
| Control | 55.65 ± 0.87$^b$ | 61.56 ± 0.45$^b$ | 66.99 ± 0.49$^b$ | 1.14 ± 0.14$^a$ | 55.28 ± 0.52$^b$ |
| RLow | 55.67 ± 1.03$^b$ | 61.85 ± 0.25$^b$ | 67.52 ± 1.03$^b$ | 1.01 ± 0.12$^a$ | 55.35 ± 0.41$^b$ |
| RHigh | 55.19 ± 0.33$_b$ | 61.99 ± 0.14$^b$ | 67.89 ± 0.73$^b$ | 0.92 ± 0.04$^b$ | 55.83 ± 1.15$^b$ |
| Maize | 64.44 ± 0.23$_a$ | 70.06 ± 0.03$^a$ | 75.45 ± 0.63$^a$ | 1.33 ± 0.01$^a$ | 61.41 ± 0.13$^a$ |

Results are presented as mean ± standard deviation of triplicate determinations. Different subscripts in each column represent significant differences ($p \leq 0.05$). $T_o$ – onset temperature; $T_p$ – peak temperature; $T_f$ – final temperature; G* – complex modulus; Control – starch isolated from unroasted wheat; RLow – starch isolated from wheat roasted at low roasting conditions; RHigh – starch isolated from wheat roasted at high roasting conditions; Maize – starch isolated from maize.

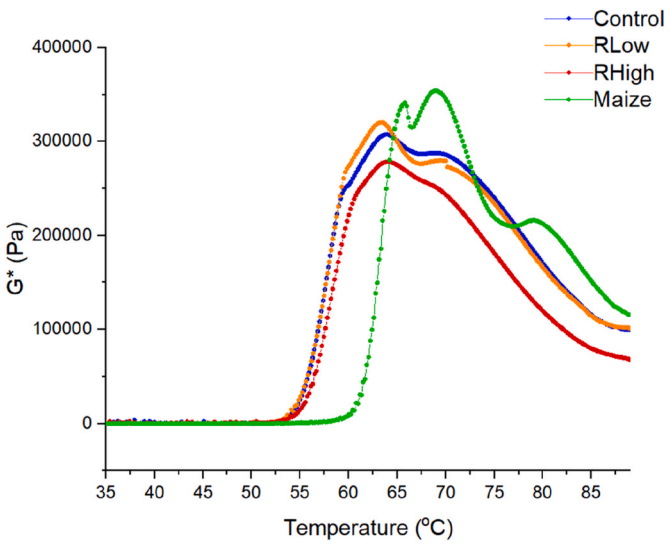


**Fig. 1.** Complex shear modulus [G*] (Pa) of starch isolated from unroasted wheat (control) and wheat roasted at low (RLow) and high (RHigh) roasting conditions, as well as maize starch at 50% moisture content as a function of a temperature ramp (5 °C/min).

### 3.2. Interpretation of TD-NMR measurements during starch gelatinisation

Transverse relaxation measurements were used to investigate gelatinisation behaviour of the starches in a 50% starch-water mixture at a constant heating rate. Generally, at intermediate moisture contents (*ca.* 40–60%), insufficient moisture is available to completely gelatinise starch (Garcia et al., 1997). It is also possible that the dry thermal treatment could have led to water evaporation from the kernel, potentially causing water compartmentalisation within the isolated wheat starch. This was reflected in the *changes in transverse relaxation times* of the NMR signal.

Once water is added to the starch during sample preparation, starch polymers undergo hydration. The degree of hydration is dependent on the accessible binding sites available for the establishment of hydrogen bonds. In the RK-ROSE signal, observations of starch crystal structure and various states of starch hydration were possible due to its occurrence within a very short timescale, making it particularly sensitive to rigid-like and solid-like structures. In contrast, the CPMG signal with longer relaxation times, allowed for the observation of the distribution of water molecules in the system. As the temperature increases, the relaxation times change according to the strength of the water-starch interaction.

The change in the relaxation times of the different proton populations during heating (later explained in Figs. 3 and 4) were not observed in previous studies that investigated the evolution $T_2$ relaxation as a function of temperature (Rondeau-Mouro et al., 2015; Kovrlija and Rondeau-Mouro, 2017a; Rakhshi et al., 2022). The use of more frequent measurements during the temperature ramp (2 °C increments from 55 to 75 °C) in the current study facilitated precise detection of the changes in mobility of hydrogen atoms linked with starch polymers and water. In contrast to the previous studies with 10 °C increments, the current approach, utilising 2 °C increments during the temperature ramp, provides a finer resolution for the detection of observed transitions (Rondeau-Mouro et al., 2015; Kovrlija and Rondeau-Mouro, 2017b). Furthermore, the total NMR signal acquisition time for this study was relatively quick compared to the 0.2 °C/min temperature ramp with 10 (Rakhshi et al., 2022) to 15 min (Rondeau-Mouro et al., 2015; Kovrlija and Rondeau-Mouro, 2017a) holding time prior to each acquisition.

*3.2.1. $T_2$* relaxation characteristics of the solid-like phase (starch-like phase)*

As previously stated, two approaches were used to process the data obtained from the RK-ROSE signal. Examples of RK-ROSE signal decay is shown in Fig. S2(a). A fraction with short relaxation time ($T_{2s}$*) were identified by removing the mobile fraction (>64 μs) in the SMA, using Equation (3). This fraction ($T_{2s}$*) followed similar oscillation behaviour during heating as observed with the Abragamian function ($T_{2(1)}$*) (Eq. (1)), but at slightly shorter times (refer to section 2.6). The exponential function used to interpret the NMR signal provided true representation of the change in relaxation times for the fast-decaying protons during heating. Fig. 2a and b depict the changes in relaxation times ($T_{2(1)}$*) and $M_2$ values during heating, respectively.

The temperature dependence of the relaxation times of different proton populations, $T_{2(i)}$*, and their corresponding amplitudes (Equation (2)), $A_i$'s are given in Fig. 3. The component of the shortest relaxation time ($T_{2(1)}$*) is referred to as the starch semicrystalline structure. The changes in its relaxation time can be understood by considering the changes observed on the $M_2$ values (Fig. 2b).

The $M_2$ of the solid fraction (<64 μs) is the weighted sum of the crystalline and amorphous lines on the wide line $^1$H NMR spectrum (Grunin et al., 2019). Therefore, the changes observed in the $M_2$ values are caused by the primary contribution of either crystalline or amorphous parts in the semicrystalline regions, with higher $M_2$ values indicating greater crystallinity. Lower $M_2$ indicates greater amorphous contribution.

The relaxation times of proton population 1 referred to as $T_{2(1)}$*, remained relatively constant from 20 to 55 °C (Fig. 2). $T_{2(1)}$* of the control and RLow samples increased significantly ($p < 0.01$) from 55 to 63 °C. We suggest proton population 1 consists of protons within the semicrystalline structure of starch, i.e., *hydrogen protons in CH groups of amylose and amylopectin.* The longer relaxation times up to 63 °C may therefore be associated with destabilisation of amylopectin structures by melting of the double helical structures, resulting in greater amorphous contribution. This is supported by the decreasing $M_2$ values (Fig. 2b) up to 63 °C of proton population 1 indicating the loss of crystalline structures (resulting in a larger amorphous part) of the semicrystalline region. As the temperature rises, the mobility of the amorphous components increases as it becomes less constrained.

Above 63 °C, shorter relaxation times is observed for the fast-decaying protons (proton population 1) and $M_2$ values also increase up to *ca.* 73 °C. Within this temperature range, the amorphous contribution decreases as observed by the reduction in $A_1$ (fraction of semicrystalline structure) (Fig. 3). Consequently, the remaining crystalline portion of the semicrystalline structure are responsible for shorter relaxation times and higher $M_2$ values, which represent a greater crystalline appearance. In this case, there is no increase in the crystalline material. It is rather the overall portion (amplitude) of this population that contributes to the signal decreases during heating. This is observed by the lowered $A_1$ values in Fig. 3. As protons become more mobile, as for instance during the breakage of double helical amylopectin polymers, they shifted to longer relaxation times, specifically in population 2 ($T_{2(2)}$*), which were detected by RK-ROSE. The portion of population 1 ($A_1$), that remained unaffected by heating, contributed to the increase in crystallinity. However, its contribution to the overall signal is minimal.

By the end of the heating cycle, at 80 °C, the fraction of the rigid component greatly decreased (Fig. 3) and ranged between 6.5 and 7.8% for wheat starch and at 10.2% for maize starch, indicating major destruction of the semicrystalline regions. The roasted wheat showed a lower final value (6.6 for RLow and 6.4% for RHigh) of the intact semicrystallne structure compared to the control wheat sample (7.8%). Despite extensive disruption, the residual fraction (at 80 °C) could potentially signify the segment that remained unaffected by heat treatment, possibly due to insufficient moisture. At 80 °C, the residual fraction remained 'ungelatinised.' Heating, for instance to 90 °C, could potentially lead to a further reduction in the fraction. Nevertheless, further experiments are required to ascertain complete gelatinisation.

Protons originating from populations 2 ($T_{2(2)}$*) and 3 ($T_{2(3)}$*) were similarly affected by the heating process (Fig. 3a). The relaxation times remained relatively constant up to 50 °C for the wheat starch and 55 °C for the maize starch. Subsequently, a significant ($p < 0.001$) increase in $T_{2(2)}$* was observed for all starches while $T_{2(3)}$* increased significantly for the control ($p < 0.05$) and the maize starch ($p < 0.001$) up to 80 °C. This was caused by increased mobility of protons due to temperature rise. Bosmans et al. (2012) also observed two populations with spin-spin relaxation times between 70 and 300 μs, detected by FID and CPMG, in unheated and heated starch-water system (47% moisture content). These populations were categorised into one proton group due to similar influence of heat treatment, namely CH protons of amorphous starch. In the present study it is evident that the shifts in proton abundance within populations 2 and 3 during heating (Fig. 3b) are attributed to the ongoing changes in the mobility of hydrogen atoms. Hence, populations 2 and 3 correspond to protons within starch molecules displaying varying degrees of hydration, with population 2 containing more

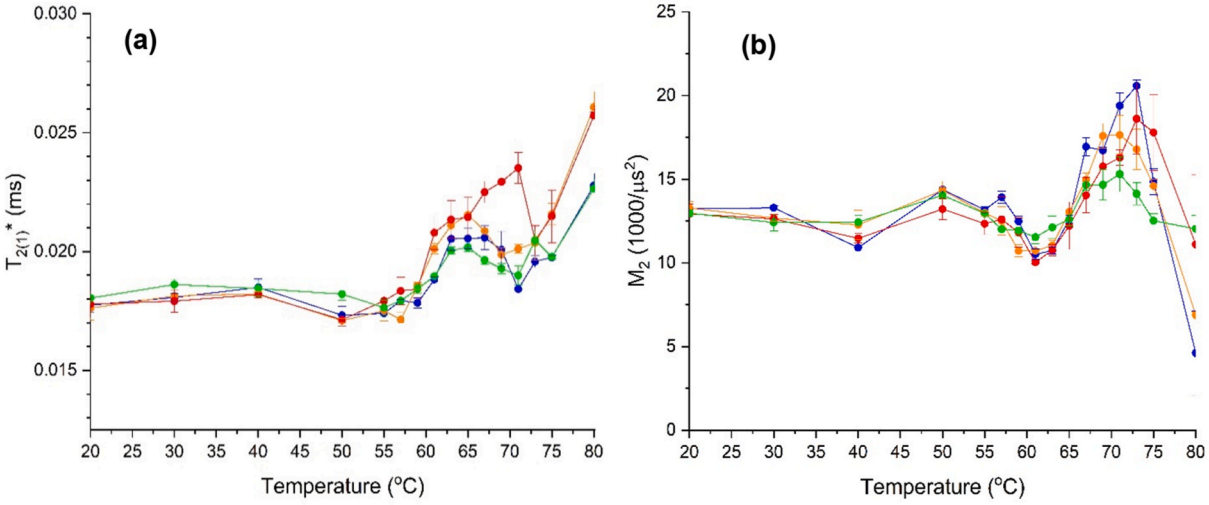


**Fig. 2.** (a) Observed transverse relaxation times of the rigid component ($T_{2(1)}$*) and (b) second moment ($M_2$) values as a function of temperature for starch isolated from unroasted wheat (blue), roasted wheat, namely RLow (orange) and RHigh (red), and maize starch (green). Results are presented as means of duplicate analysis with error bars indicating standard error.

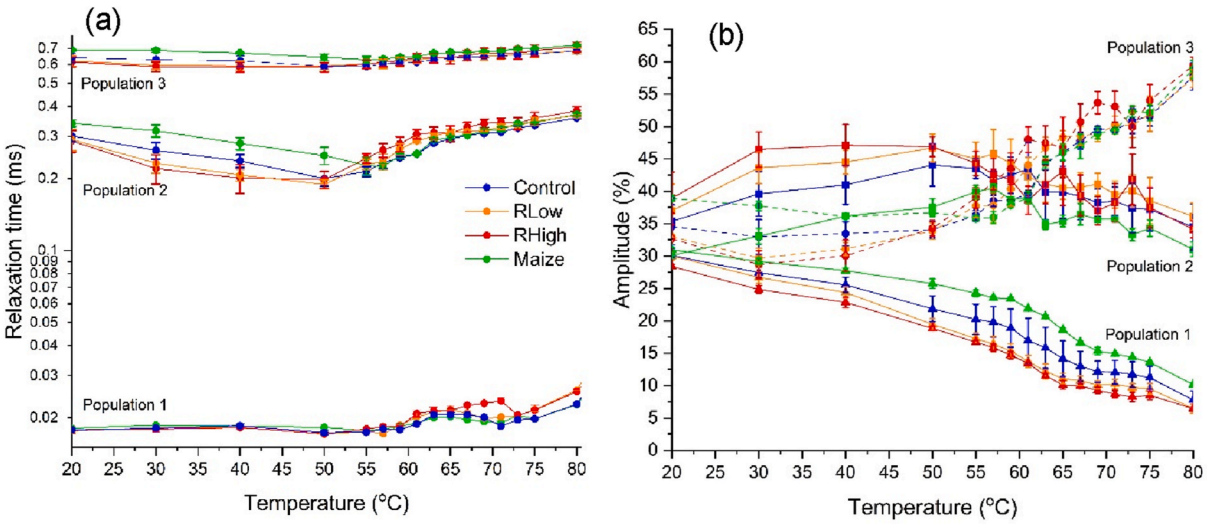


**Fig. 3.** (a) Observed transverse relaxation times and (b) associate normalised amplitudes of the first, second and third proton populations detected by RK-ROSE sequence of the hydrated starch isolated from unroasted wheat (blue), roasted wheat, namely RLow (orange) and RHigh (red), and maize starch (green) as a function of temperature. Results are presented as means of duplicate analysis with error bars indicating standard error.

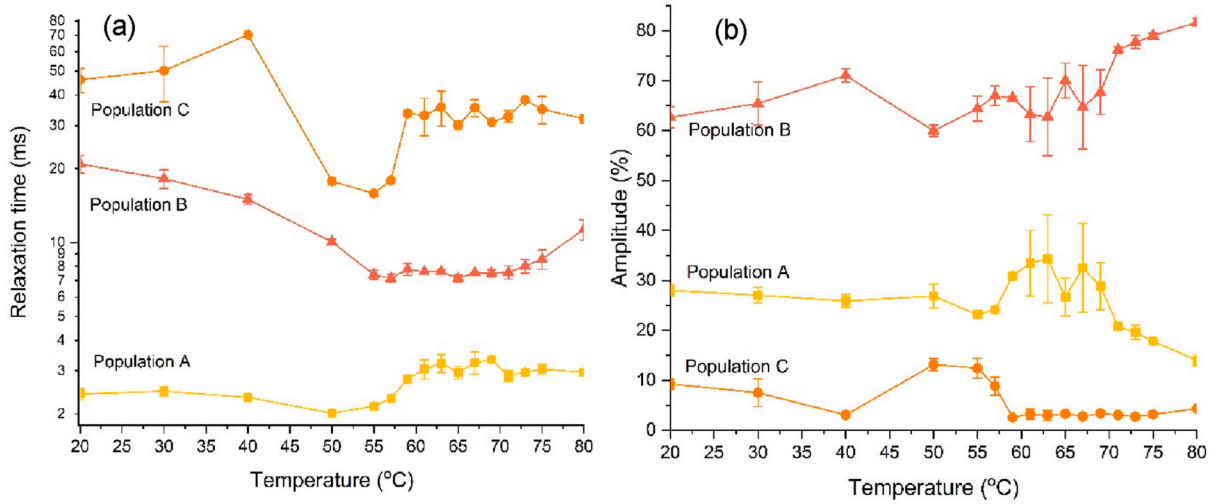


**Fig. 4.** (a) Spin-spin relaxation times and (b) normalised amplitudes of the corresponding relaxation contributions A (—■—), B (—▲—) and C (—●—) in liquid-like phase (water-like) as a function of temperature of hydrated wheat starch (RLow wheat starch; 50% moisture content). Results presented as mean of duplicate analysis with error bars indicating standard error.

structured zones characterises by lower hydration levels. Throughout the heating cycle, the abundance of population 3 increased due to the enhanced mobility of protons within populations 1 and 2. Consequently, there was a shift towards the population with longer relaxation times, i.e. protons shifted from populations 1 and 2 to population 3. As population 2 has shorter relaxation times, compared to population 3, it indicates that the structure is more rigid, thus it has more 'structured zones'.

For the starch isolated from the roasted wheat samples, the abundance of protons in population 3, up to 40 °C, were higher compared to the starch from unroasted wheat and maize samples. This confirms that roasting induced starch damage and therefore an increase in the amorphous content (Schoeman and Manley, 2019). Maize starch, compared to the wheat starches, had the largest contribution of protons within population 2 up to 50 °C. This is possibly associated with more rigid or structured-like zones. The higher temperatures observed for the onset of gelatinisation for maize (*ca.* 64 °C), compared to wheat (*ca.* 55 °C) starch (Table 1) support these findings.

### 3.2.2. *Transverse relaxation characteristics of the liquid-like phase (water-like)*

The magnetisation curves obtained by applying CPMG pulse sequence (Fig. S2b) were analysed according to Eq. (4). Fig. 4 illustrates the variation in $T_2$ relaxation times and the corresponding normalised amplitudes during the temperature increase for RLow wheat starch. A similar trend was observed for all starch samples (depicted in Fig. S3). CPMG pulse sequence was used to determine the distribution of water within the starch-water system. During heating the relaxation time for population A remained relatively constant with a slight increase after 50 °C for the wheat starch samples and 59 °C for the maize starch in the present study. The amplitude of the relaxation contribution associated with population A decreased throughout the heating cycle to a final value in the range of 12.5–12.8% for all samples (15.4% loss for the control, 15.5% for RLow, 15% for RHigh and 14% for maize). This was accompanied with increasing amplitude of proton population B. The overall reduction in amplitude and increase in relaxation time of population A during heating was likely due to the leaching of amylose from

the granules. Population A is consequently linked to hydrogen atoms of intragranular water protons bound to starch, aligning with the findings of Kovrlija and Rondeau-Mouro (2017b).

The CPMG signal predominantly reflects the contribution associated with the intermediate relaxation time, constituting approximately 58–62% for all samples, with an increase of around 20% observed during heating. The impact of the temperature ramp on the relaxation time of proton population B was characterised by an initial decrease, followed by stabilisation and subsequent increase in relaxation times (Fig. 5). Kovrlija and Rondeau-Mouro (2017b) attributed this relaxation process to extra granular water protons forming strong interactions with starch. $T_{2(B)}$ showed a significantly decrease ($p < 0.0001$) between 20 and 55 °C for the wheat starch samples and from 20 to 61 °C for the maize starch (Fig. 5). The reduced $T_{2(B)}$ relaxation times, due to reduced mobility, result from water molecules diffusing into the amorphous regions, where they form strong interactions with starch.

The $T_{2(B)}$ relaxation times stabilised from 55 to 75 °C and from 61 to 80 °C for the wheat and maize samples, respectively. These initial temperatures of stabilisation aligned with the gelatinisation onset temperatures as measured by DSC and the temperatures associated with initial increase of G* (Table 1). During this time interval, starch granules absorb moisture and swell. The increase in viscosity associated with gelatinisation therefore occurred during the stabilisation phase and was not observed by a change in relaxation time. This viscosity/stiffness increase, which reduces molecular mobility (Bosmans et al., 2012), could not be observed by population B, the most abundant component.

RHigh exhibited longer $T_{2(B)}$ relaxation times during stabilisation compared to the other wheat starch samples, and significantly longer ($p < 0.05$) times at 55 °C compared to RLow. A similar trend was observed for the control sample at 61 to 67 °C. This corresponds with the lower stiffness (lower G*) observed for RHigh due to roasting, as indicated by the intensity of the complex modulus in Fig. 1, compared to the other wheat starch samples. In contrast, the maize starch exhibited the longest $T_{2(B)}$ relaxation times (Fig. 5) corresponding with the highest firmness (Fig. 1). As discussed in Section 3.1, it should be kept in mind that the maximum stiffness between maize and wheat starches cannot be compared directly. The viscoelastic properties of starches of different sources can vary due to their different physical properties (Kilbride et al., 2019). Nevertheless, when comparing starch from similar sources, lower $T_{2B}$ relaxation times could serve as indicators of higher maximum stiffness during gelatinisation, implying greater water holding capacity, i.e., *stronger interaction between starch and water.*

Finally, population C is associated with limited interaction between extra granular water protons and starch, referred to as the 'lesser starch-rich water phase' (Kovrlija and Rondeau-Mouro, 2017a). Due to the very low amplitudes (abundance of protons) of population C in the liquid phase during temperature rise, experimental variations in relaxation times of this population were observed. Stronger starch-water interactions were observed during heating, from 55 °C for wheat and 61 °C for maize, indicated by the lowered $T_{2(C)}$ relaxation times.

## 4. Conclusion

Through temperature ramp experiments, TD-NMR analysis was successfully used to illustrate changes in the crystalline and amorphous components of wheat and maize starch. The 2 °C temperature increments (from 55 to 75 °C) used enabled ~~more~~ detailed detection of the changes in mobility of hydrogen atoms associated with starch polymers and water. This approach provided results that align with the corresponding findings obtained through DSC and rheological tests. The second moment and the relaxation time of the pool of protons with fastest relaxation behaviour from the RK-ROSE signal, provided information on the extent of gelatinisation of the semicrystalline structure at 80 °C. In addition, information on the crystal structure state during heating, i.e., greater amorphous contribution at gelatinisation temperatures (up to 63 °C) was observed. Furthermore, maize starch had the greatest level of semicrystalline structure intact at the end of the heating cycle, while the starches isolated from the roasted wheat were the lowest. The CPMG signal was decomposed to obtain information on the distribution of water protons bound to starch. Gelatinisation onset temperature was observed by the change in $T_2$ of the most abundant component, population B. DSC tests showed similar gelatinisation temperatures for the starches. It was confirmed that roasting affected the viscoelastic properties of starch by reducing the maximum stiffness during gelatinisation, as also observed by longer relaxation times of population B at similar temperatures. Changing the moisture content of starch solutions could be considered for future studies. TD-NMR was shown to be an effective and simple method to perform crystallinity measurements and study starch gelatinisation.

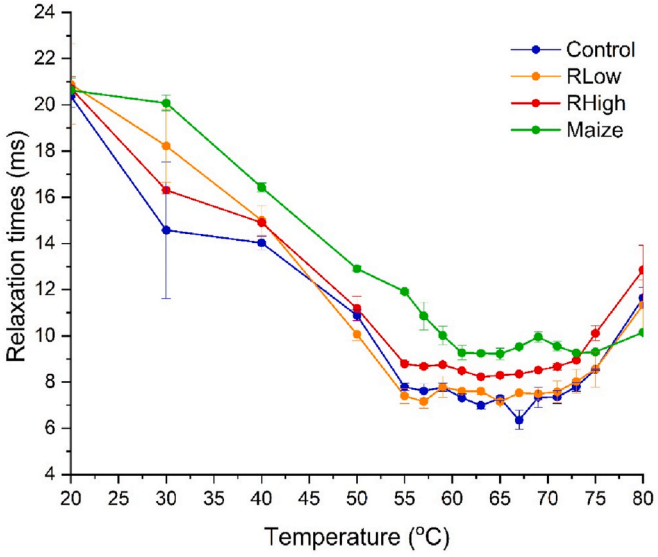


**Fig. 5.** $^1$H transverse relaxation times of population B for starch isolated from unroasted wheat, roasted wheat, namely RLow and RHigh, and maize starch as a function of temperature. Results presented as mean of duplicate analysis with error bars indicating standard error.

## Funding

This study has received funding from the European Union's Horizon 2020 Research and Innovation programme – MSCA RISE under grant agreement # 10100822.

## CRediT authorship contribution statement

**Jana van Rooyen:** Writing – review & editing, Writing – original draft, Methodology, Investigation, Formal analysis, Conceptualization. **Leonid Grunin:** Writing – review & editing, Resources, Methodology, Conceptualization. **Mecit Oztop:** Writing – review & editing, Resources, Methodology. **Danuta Kruk:** Writing – review & editing. **Marena Manley:** Writing – review & editing, Supervision, Conceptualization.

## Declaration of competing interest

The authors declare no conflict of interest. Dr. Leonid Grunin is the official partner of the project and representing the Resonance Systems GmBH in the project. Thus, there is no conflict of interest among partners as this is an outcome of the EU project.

## Data availability

Data will be made available on request.

## Acknowledgements

Jana van Rooyen acknowledged the Postgraduate Scholarship Programme (PSP) from Stellenbosch University, South Africa for study grant provided.

## Appendix A. Supplementary data

Supplementary data to this article can be found online at https://doi.org/10.1016/j.jfoodeng.2024.112041.

## References

AACC, International, 2010. Method 26-95.01 and method 26-50.01. Approved methods of analysis, 11th ed.
Bertoft, E., 2017. Understanding starch structure: recent progress. Agronomy 7.
Bosmans, G.M., Delcour, J.A., 2017. Modern Magnetic Resonance. *Modern Magnetic Resonance*.
Bosmans, G.M., Lagrain, B., Deleu, L.J., Fierens, E., Hills, B.P., Delcour, J.A., 2012. Assignments of proton populations in dough and bread using NMR relaxometry of starch, gluten, and flour model systems. J. Agric. Food Chem. 60, 5461–5470.
Choi, S.G., Kerr, W.L., 2003. 1H NMR studies of molecular mobility in wheat starch. Food Res. Int. 36, 341–348.
Delcour, J.A., Hoseney, R.C., 2010. Principles of Cereal Science and Technology, third ed. AACC International, St. Paul, MN.
Duynhoven, J. van, Voda, A., Witek, M., As, H. Van, 2010. Time-domain NMR applied to food products. In: Webb, G.A. (Ed.), Annual Reports on NMR Spectroscopy. Elsevier Ltd, pp. 145–197.
Garcia, R.H.S., Filgueiras, J.G., deAzevedo, E.R., Colnago, L.A., 2019. Power-optimized, time-reversal pulse sequence for a robust recovery of signals from rigid segments using time domain NMR. Solid State Nucl. Magn. Reson. 104, 101619.
Garcia, V., Colonna, P., Bouchet, B., Gallant, D.J., 1997. Structural changes of cassava starch granules after heating at intermediate water contents. Starch/Staerke 49, 171–179.
Grunin, L., Ivanova, M., Schiraya, V., Grunina, T., 2023. Time-domain NMR techniques in cellulose structure analysis. Appl. Magn. Reson. 54, 929–955.
Grunin, L., Oztop, M.H., Guner, S., Baltaci, S.F., 2019. Exploring the crystallinity of different powder sugars through solid echo and magic sandwich echo sequences. Magn. Reson. Chem. 57, 607–615.
Kilbride, P., Rull, M.V., Townsend, A., Wilson, H., Morris, J., 2019. Shear-thickening fluids in biologically relevant agents. Biorheology 56, 39–50.
Kim, K.H., Kim, J.Y., 2021. Understanding wheat starch metabolism in properties, environmental stress condition, and molecular approaches for value-added utilization. Plants 10.
Kovrlija, R., Goubin, E., Rondeau-Mouro, C., 2020. TD-NMR studies of starches from different botanical origins: hydrothermal and storage effects. Food Chem. 308, 125675.
Kovrlija, R., Rondeau-Mouro, C., 2017a. Hydrothermal changes of starch monitored by combined NMR and DSC methods. Food Bioprocess Technol. 10, 445–461.
Kovrlija, R., Rondeau-Mouro, C., 2017b. Hydrothermal changes in wheat starch monitored by two-dimensional NMR. Food Chem. 214, 412–422.
Kulkarni, V.S., Shaw, C., 2016. Rheological Studies. Essential Chemistry for Formulators of Semisolid and Liquid Dosages. Elsevier.
Maus, A., Hertlein, C., Saalwächter, K., 2006. A robust proton NMR method to investigate hard/soft ratios, crystallinity, and component mobility in polymers. Macromol. Chem. Phys. 207, 1150–1158.
Pauly, A., Pareyt, B., Brier, N. De, Fierens, E., Delcour, J.A., 2012. Starch isolation method impacts soft wheat (Triticum aestivum L. cv. Claire) starch puroindoline and lipid levels as well as its functional properties. J. Cereal. Sci. 56, 464–469.
Rakhshi, E., Cambert, M., Diascorn, Y., Lucas, T., Rondeau-Mouro, C., 2022. An insight into tapioca and wheat starch gelatinization mechanisms using TD-NMR and complementary techniques. Magn. Reson. Chem. 60, 702–718.
Riley, I.M., Ooms, N., Delcour, J.A., 2022. The use of time domain 1 H NMR to study proton dynamics in starch-rich foods : a review. Compr. Rev. Food Sci. Food Saf. 1–38.
Rondeau-Mouro, C., Cambert, M., Kovrlija, R., Musse, M., Lucas, T., Mariette, F., 2015. Temperature-associated proton dynamics in wheat starch-based model systems and wheat flour dough evaluated by NMR. Food Bioprocess Technol. 8, 777–790.
van Rooyen, J., Delcour, J.A., Oyeyinka, S.A., Simsek, S., Kidd, M., Manley, M., 2023a. Prior roasting of wheat impacts on the functionality of flour prepared from it: Part 1. Wheat flour viscosifying properties. Cereal Chem. 1–14.
van Rooyen, J., Delcour, J.A., Oyeyinka, S.A., Simsek, S., Kidd, M., Manley, M., 2023b. Prior roasting of wheat impacts on the functionality of flour prepared from it: Part 2. Wheat protein functionality. Cereal Chem. 1–10.
van Rooyen, J., Marini, F., Orth, S.H., Oyeyinka, S.A., Simsek, S., Manley, M., 2023c. Effect of wheat roasting conditions and wheat type on short-wave infrared (SWIR) spectral data of whole and milled wheat by ANOVA-simultaneous component analysis. Spectrochim. Acta Mol. Biomol. Spectrosc. 303, 123160.
van Rooyen, J., Simsek, S., Oyeyinka, S.A., Manley, M., 2022. Holistic view of starch chemistry, structure and functionality in dry heat-treated whole wheat kernels and flour. Foods 11, 207.
Schoeman, L., Manley, M., 2019. Oven and forced convection continuous tumble (FCCT) roasting: effect on physicochemical, structural and functional properties of wheat grain. Food Bioprocess Technol. 12, 166–182.
Schoeman, L., Plessis, A. Du, Manley, M., 2016. Non-destructive characterisation and quantification of the effect of conventional oven and forced convection continuous tumble (FCCT) roasting on the three-dimensional microstructure of whole wheat kernels using X-ray micro-computed tomography (μCT). J. Food Eng. 187, 1–13.
Shi, Y.C., Capitani, T., Trzasko, P., Jeffcoat, R., 1998. Molecular structure of a low-amylopectin starch and other high-amylose maize starches. J. Cereal. Sci. 27, 289–299.
Vamadevan, V., Bertoft, E., 2020. Observations on the impact of amylopectin and amylose structure on the swelling of starch granules. Food Hydrocolloids 103, 105663.